

**A Novel Method for Quantifying Uncertainty in the Unified
Envelope of Constraint in the Passive Knee Joint**

By

Andrew M. Boppart

Submitted to the graduate degree program in Bioengineering and the Graduate Faculty of the
University of Kansas in partial fulfillment of the requirements for the degree of Master of
Science

Dr. Lorin Maletsky, Chairperson

Dr. Lisa Friis, Committee Member

Dr. Sara Wilson, Committee Member

Date Defended: 27 November 2018

The Thesis Committee for Andrew M. Boppart
certifies that this is the approved version of the following thesis

**A Novel Method for Quantifying Uncertainty in the Unified
Envelope of Constraint in the Passive Knee Joint**

Dr. Lorin Maletsky, Chairperson

Date Approved: 30 November 2018

Abstract

The Experimental Joint Biomechanics Research Lab at the University of Kansas created the unified envelope (UE) of constraint as a means for describing the overall laxity of the passive knee joint. The UE is currently calculated with the use of a radial basis function (RBF), which has been shown to provide a useful approximation of the multidimensional relationship between applied forces and observed kinematics. However, the UE does not provide any information regarding its certainty in the approximation at any given position, making comparisons between UEs more difficult. The main objective of this thesis was to create an estimate for the uncertainty of the UE, specific to each point within the UE. Secondary objectives included reducing the effect of the investigator on the UE and determining the optimal protocol for loading during laxity evaluations. To determine if the proposed method was able to meet the objectives, three different investigators performed manual laxity evaluations on one cadaveric specimen. Data from these evaluations were sequentially downsampled and used to create many slightly different UEs. The variance of these UEs at each point were combined with a general measure of variance, found by calculating the variance of the error when RBFs use the sequentially downsampled data to approximate known data. This estimate appeared to perform well throughout the envelope, providing a standard deviation consistent with measurements from previous studies. Results also showed a decrease in the median absolute difference between investigators of 18.3% in VV°, 15.6% in IE°, and 16.2% in AP position (mm) when compared to the previous method. The importance of collecting both uniaxial and multiaxial loading trials during the laxity evaluation was also verified. The following chapters provide further information on methods and results, along with future applications.

Table of Contents

Abstract	iii
List of Tables	v
List of Figures	vi
Chapter 1: Introduction	1
Chapter 2: Literature Review	3
Chapter 3: A Novel Method for Quantifying Uncertainty in the Unified Envelope of Constraint in the Passive Knee Joint	8
3.1 Abstract	8
3.2 Introduction	9
3.3 Methods	11
3.4 Results	16
3.4.1 Visualizing the UE in 3D	16
3.4.2 Uniaxial Loading vs Multiaxial Loading	17
3.4.3 Comparing investigators and methods	18
3.4.4 Standard Deviation and Significant Differences	19
3.5 Discussion	20
3.6 Tables	24
3.7 Figures	26
Chapter 4: Conclusion.....	37
References.....	40

List of Tables

Table 1: Number of paths and data points by each investigator and loading type 24

Table 2: Values for the calculated variance from the RBFs, the observed variance from the difference between predicted and measured values, and the difference between the two used to uniformly shift the variance from the RBFs up to match the observed variance. 24

Table 3: Average MAD of SDS-UEs and average percent of the SDS-UE that is significantly different (two-tailed t-test, $p < 0.05$) between investigators separated by dependent variable and type of loading used to train RBF. 24

Table 4: Median absolute difference of UEs between investigators at every grid point of the UE when using both the previous method and the SDS Method along with the relative percent decrease in median absolute difference from the previous method to the SDS method..... 25

Table 5: Minimum (0th Percentile), median (50th Percentile), and maximum (100th Percentile) values for standard deviation for each investigator and output. 25

List of Figures

Figure 1: Manual laxity evaluation setup [35]..... 26

Figure 2: LabVIEW Interface providing near real-time feedback for laxity evaluations. Square color would change as more data were collected within each square, black means no data has been collected in that region. 27

Figure 3: RBF flowchart. Experimental data is used to determine the weight of each experimental point, then the weights are used to estimate dependent variables through a generic, evenly spaced grid [26]. 28

Figure 4: Example of predictions made for one experimental point at 30.1° Flexion, -1.9Nm VV torque, -5.6Nm IE torque, and 6.2N AP force. All four downsampling cases are included with the 5 predictions made from every 5th point in magenta, 10 predictions from every 10th point in blue, 20 predictions from every 20th point in cyan, and 40 predictions from every 40th point in green. Included are the four means ± 1 standard deviation of each downsampling case. The red dot is the mean of the four downsampling case means ± 1 standard deviation and the black dot is the measured value that was being predicted. 29

Figure 5: Power spectral density and cumulative power spectral density for one laxity evaluation trial with VV torque and IE torque applied by investigator 1. Cumulative power spectral density chart is showing cumulative power from 0.9 to 1 and frequency from 0 to 5 Hz to help differentiate between variables. Two other lines are included, one horizontal line at 99% cumulative power and one vertical line at a frequency of 2.5 Hz, to show that over 99% of the power in all signals are contained in frequencies below 2.5 Hz (every 40th point from a 100Hz signal). 30

Figure 6: Investigator 1’s UE calculated using the SDS method represented by isosurface renderings at constant load magnitudes, scaled by their respective maximums (16 Nm of VV torque and 6 Nm of IE torque). The blue surface is at 100% magnitude and the red surface is at 50%. **A:** Data between 30° and 50° flexion is omitted for visualization. **B:** Data with an external load is omitted for visualization. **C:** Data with a Valgus load is omitted for visualization. 31

Figure 7: Investigator 1’s SDS-UE trained with only uniaxial loading trials shown in red, and trained with only multiaxial loading trials shown in black. Top row has VV kinematics vs flexion angle at -100% (left), 0% (center), and 100% (right) applied IE torque (-6 Nm, 0 Nm, 6 Nm). The lines in the top row correspond to applied VV torques at -100% (bottom line, -16 Nm), -50%, 0% (center line, 0 Nm), 50%, and 100% (top line, 16 Nm). Bottom row shows IE kinematics vs flexion angle at -100% (left), 0% (center), and 100% (right) applied VV torque (-16 Nm, 0 Nm, 16 Nm). The lines in the bottom row correspond to applied IE torques at -100% (bottom line, -6 Nm), -50%, 0% (center line, 0 Nm), 50%, and 100% (top line, 6 Nm)..... 32

Figure 8: Range of all Investigators UEs calculated with the previous method shown in red and the SDS method in blue, areas with overlap are colored purple. Top row has VV kinematics vs flexion angle at -100% (left), 0% (center), and 100% (right) applied IE torque (-6 Nm, 0 Nm, 6 Nm). The lines in the top row correspond to applied VV torques at -100% (bottom line, -16 Nm), -50%, 0% (center line, 0 Nm), 50%, and 100% (top line, 16 Nm). Bottom row shows IE kinematics vs flexion angle at -100% (left), 0% (center), and 100% (right) applied VV torque (-16 Nm, 0 Nm, 16 Nm). The lines in the bottom

row correspond to applied IE torques at -100% (bottom line, -6 Nm), -50%, 0% (center line, 0 Nm), 50%, and 100% (top line, 6 Nm). 33

Figure 9: Average of all investigators SDS-UE at 100% load magnitude colored by overall standard deviation quartile of all variables and investigators (i.e. the percentile of VV standard deviation, IE standard deviation, and AP standard deviation for I1, I2, and I3 was found at each grid point of the SDS-UE. The overall standard deviation quartile was found by averaging these nine standard deviation percentiles). 34

Figure 10: Investigator 1’s UE at 100% load magnitude colored by how much it differs in VV° from Investigator 2’s UE at 100% load magnitude. **A:** Previous method for the UE was used for the plot and in the difference calculation for color. **B:** SDS method for the UE was used for the plot, in the difference calculation, and to determine significance. Only significant differences are colored (one-tailed t-test, $p < 0.2$). **C:** Same as plot B with $p < 0.05$ rather than $p < 0.2$ 35

Figure 11: Investigator 1’s UE at 100% load magnitude colored by how much it differs in IE° from Investigator 2’s UE at 100% load magnitude. **A:** Previous method for the UE was used for the plot and in the difference calculation for color. **B:** SDS method for the UE was used for the plot, in the difference calculation, and to determine significance. Only significant differences are colored (one-tailed t-test, $p < 0.2$). **C:** Same as plot B with $p < 0.05$ rather than $p < 0.2$ 36

List of Abbreviations

ACL	Anterior Cruciate Ligament
AP	Anterior-Posterior
DOFs	Degrees of Freedom
EJBRL	Experimental Joint Biomechanics Research Lab
I1	Investigator 1
I2	Investigator 2
I3	Investigator 3
IE	Internal-External
MAD	Median Absolute Difference
RBF	Radial Basis Function
SDS	Sequential Downsample
SDS-UE	Unified Envelope found from sequentially downsampled data
UE	Unified Envelope
VV	Varus-Valgus

Chapter 1: Introduction

The passive knee joint has been studied extensively in the past to form a better understanding of the complex relationship between the different anatomical structures of the knee joint [1]. The constraint of the knee is a result of multiple anatomical structures working together to allow the knee both translational and rotational freedom of motion [2]. In the past, methods for measuring this constraint have generally been limited to the application of a single force followed by a measurement of relative displacement in the direction the force was applied.

More recent work, performed in the Experimental Joint Biomechanics Research Lab at the University of Kansas has attempted to describe multiple degrees of freedom (DOF) at the same time, using radial basis functions to develop the unified envelope (UE) of constraint. The UE has been shown to be a valuable measure, and has been applied to research involving the contribution of individual ligaments to overall constraint and has helped develop and verify computational models of the knee. Currently, the UE describes the knee with exact positions at each applied force and is limited by its inability to comment on confidence in the reported position. This limits its application and makes comparisons between UEs more difficult.

The main goal of this research was to develop a measure of the uncertainty in the unified envelope. There were also two secondary goals that focused on more general improvements to the unified envelope. The first of these was to make the UE more robust by reducing the effect the investigator has on the final result. The second goal was to determine the best protocol for data collection during laxity evaluations by comparing UEs calculated from different loading protocols.

Chapter 2 provides a review of the current literature, providing background on joint laxity assessments, radial basis functions, and the work done by the Experimental Joint Biomechanics Research Lab at the University of Kansas. Chapter 3 presents a study with a method for quantifying uncertainty in the UE and provides information on how well the method works. Chapter 4 has the conclusions of the research and applications for the knowledge gained from this thesis.

Chapter 2: Literature Review

The laxity of the passive knee joint has been studied for decades by dozens of authors to help understand how the anatomy of the knee affects overall joint constraint [1]. Laxity of the knee is defined as the displacement of the tibia relative to the femur when transitioning from an unloaded to a loaded state, and the knee joint is considered passive when there is no muscle activation affecting motion. Laxity evaluations have been commonly performed both clinically and in research labs to describe the behavior of the passive knee joint. A laxity evaluation is performed by measuring the change in position of the tibia relative to the femur when a load or torque is applied. Research involving laxity evaluations are generally performed *in vitro* to completely remove muscle activation, but clinical laxity evaluations must be *in vivo*. Clinical laxity evaluations are usually performed with the goal of diagnosing injuries, like torn ligaments [3,4], or when balancing the ligaments after a total knee replacement [5]. Early methods for evaluating knee laxity were performed manually and were more qualitative than many methods used today [6]. This review describes methods for performing laxity evaluations along with the accuracy and consistency of some of these methods.

The first manual method for evaluating knee laxity was the anterior drawer test [7], which was first described as early as 1879 [8]. This method was used to diagnose a torn ACL by qualitatively comparing the motion of the injured knee to the healthy knee. Another qualitative test started being used in the 1970's called the Lachman's test. The Lachman's test has been shown to be more sensitive and specific than the anterior drawer test [9], but it still relies on qualitatively comparing the injured knee to the healthy knee. Later clinical devices, such as the

Rolimeter, KT-1000, and KT-2000, have attempted to quantify the Lachman's test, but these devices are primarily used as diagnoses tools, rather than laxity evaluations [10,11].

An objective measurement of the properties of the passive knee joint has long been a goal of researchers. Methods for controlling loads have included direct manipulation [12], instrumented handlebars [13], and Instron loading devices [14]. The motions of the knee have been measured with Roentgen stereophotogrammetry [15], triaxial electrogoniometers [15], and 6 degree of freedom (DOF) instrumented spatial linkages [16]. These methods, along with the introduction of the Grood and Suntay joint coordinate system as a standard for reporting motions, greatly improved the understanding of the passive knee joint *in vitro* [17].

Most research performed before the 1980s focused on measuring a specific behavior for many specimens, rather than measuring a range of behaviors for an individual specimen. To address this limitation, Blankevoort et al. developed a rig in 1988 that would give the knee 6 DOFs while applying several combinations of external loads and torques at different flexion angles [1]. Blankevoort called this the passive envelope of motion, and it provided a quantitative way to consistently and repeatedly evaluate knee laxity under a variety of different conditions. This method could be used outside of the clinic to compare differences between knees and quantify the contribution of different ligaments to the overall constraint of the knee [18]. Blankevoort's method was an improvement over other knee laxity evaluation tools at the time, but operation was very time consuming and required a complicated rig to be built before any knee laxity evaluations could be performed.

Many devices to measure knee laxity have been introduced since Blankevoort's work on the passive envelope. The most common device currently used in both research and the clinic is the KT-2000 [19]. The KT-2000 is both simple to use and well-studied, but it only measures AP

motion at one flexion angle. To fully understand the complex joint structures and ligament interactions, laxity must be evaluated in multiple DOFs [2]. A new device was designed to measure the knee in four DOFs (flexion angle, internal-external rotation, medial-lateral translation, and anterior-posterior translation) *in vivo*, and preliminary cadaveric studies have demonstrated proficiency in measuring clinical laxity tests [20]. However, this device has a relatively high cost and would require more research before it is considered a reliable tool.

A protocol was developed at the University of Kansas Experimental Joint Biomechanics Research Laboratory (EJBRL) to address limitations found in other knee laxity studies. The protocol was designed to allow for loading and movement in 6 DOF with the goal of describing how the knee responds to multidirectional loading throughout the range of flexion. This protocol was performed by rigidly mounting the femur in an inverted-vertical position, and then manually applying external loads and torques, measured by a load cell, to the distal end of the tibia [21]. Like Blankevoort's method, this protocol allowed the knee to move in 6 DOFs and measured performance with multiaxial loading. Blankevoort's rig, however, was limited to only measuring a few different load magnitudes at specific and controlled flexion angles, while this new protocol allowed for the application of almost any load or combination of loads to be measured and approximated throughout the full range of flexion. This protocol provided a more detailed description of the passive knee joint [22], but was mostly limited to visualizing the effect of a load or torque in only one direction with respect to flexion angle, and couldn't interpolate very well if the data set was too scattered or sparse. To address these limitations radial basis functions (RBF) were introduced to describe multiple DOFs simultaneously [23]. RBFs have been shown to outperform other approximation methods, such as splines or polynomials, when data sets have many dimensions or when the distribution is non-uniform or scattered [24,25]. This method

provided a way to approximate how the knee would behave with any kind of loading at any flexion angle, or under specific loading conditions without the need to directly measure those conditions. For example, one of the loading configurations from Blankevoort's rig could be approximated with an RBF without the need to build the rig and collect data from that exact configuration. This ability to predict any position from a given set of loads made it possible to compare knees through any range of flexion angles and applied loads, a task that was previously only possible with direct measurements of both knees. Descriptions and visualizations of the behavior of the knee in more than two dimensions was now possible as well [26].

While RBFs allowed for more comparisons to be made between the passive envelope of motion of different knees, it was unclear whether these observed differences were meaningful or not. To comment on whether or not observed differences may be significant, some measure of uncertainty in the RBF approximation is necessary. Some methods have been proposed for estimating the uncertainty in the approximations of RBFs, such as counting the number of training points within an n-dimensional sphere of the point being approximated [27], but these methods are primarily measures of how much the RBF is extrapolating, rather than how accurate the extrapolation is. When estimating just uncertainty, there are many different steps in the process where it can arise. First, there is uncertainty in the tools used for data collection. The Optotrak 3020 camera system has been shown to have a standard deviation of 0.10 mm when measuring a 10 mm translation [28]. There is also uncertainty in the calculation of Grood and Suntay kinematics based on the position of probed bony anatomical landmarks [29]. Uncertainty in the repeatability of measurements between investigators has been estimated to be 0.1° - 0.2° for varus-valgus rotations and 0.3° - 0.4° for internal-external rotations [22]. Finally, the RBF approximation has been shown to be robust to both random and clustered decimation of training

data, with an average normalized root mean squared error below 2% and 2.6% respectively for all DOFs [26].

Along with no measure for uncertainty, one of the biggest limitations still present in the work done by EJBRL is the lack of compressive load control. Compressive loads have been shown to significantly affect measurements of laxity [30], and incorporating a compressive load into the laxity evaluations or into the calculation of the UE could help decrease uncertainty. However, a measure for uncertainty would need to be developed before research could be done on how to minimize it. The uncertainty in the path dependency of the knee and in the ability of the RBF to approximate known data along each loading path has yet to be studied.

Chapter 3: A Novel Method for Quantifying Uncertainty in the Unified Envelope of Constraint in the Passive Knee Joint

3.1 Abstract

The unified envelope (UE) of constraint has been proposed as a way to describe the overall laxity of the passive knee joint. The UE is currently calculated with the use of a radial basis function, which has been shown to provide a useful approximation of the multidimensional relationship between applied forces and observed kinematics. However, the UE does not provide any information regarding its certainty in the approximation at any given position, making comparisons between UEs more difficult. The primary goal of this paper was to develop a measure of uncertainty in the UE, specific to each point within the UE, that could be used to estimate how significant any observed differences may be. Other objectives included reducing the investigator's effect on the UE and determining the best protocol for loading during laxity evaluations. Manual laxity evaluations were performed by three investigators on one cadaveric specimen and used to calculate an estimate for the variation in calculated position throughout the envelope. Depending on investigator, applied forces, and flexion angle, the estimate for standard deviation ranged from 0.24° - 0.58° VV, 0.92° - 2.57° IE, and 0.31mm - 0.98mm AP. Results showed a decrease in the median absolute difference between investigators of 18.3% in VV angle difference, 15.6% in IE angle difference, and 16.2% in AP position when compared to the previous method. The importance of collecting both uniaxial and multiaxial loading trials during the laxity evaluation was also verified. Future studies could apply this method to further research on the knee, the constraint of other joints, or incorporating a measure of uncertainty into RBFs.

3.2 Introduction

The performance and stability of the active knee joint has been shown to be a function of both the anatomy of the knee and the applied forces. To improve the understanding of the constraint provided by the anatomical structures, past research has focused on studying the laxity of the passive knee joint [1]. Knee laxity is essentially how much the knee joint is displaced under a load at a flexion angle, without muscle activation. The displacement observed with the application of a load is a function of both the articular geometry and the soft tissue structures around the knee and excessive knee laxity has been shown to be associated with less stability in the joint, recurrent dislocations, and inflammatory arthritis [31]. Laxity evaluations are commonly used in academic research, but also help inform models of the joint [32,33] and can be used clinically [5]. Clinical laxity evaluations have traditionally been qualitative comparisons between an affected knee and healthy knee for the same subject with the primary goal of diagnosing injuries, usually involving torn ligaments [7,34]. Newer devices are more quantitative, and generally work by applying a load in one direction, and then measuring the displacement in that direction [6,19]. These devices are still used mainly for diagnoses [9] and usually simplify their description of the knee to only one or two degrees of freedom (DOF) [11].

Describing the laxity of the knee in only two dimensions (i.e. flexion angle vs IE rotation) does not fully capture the complex, multidimensional constraint of the joint [2]. To combat this problem, radial basis functions (RBF) have been proposed as a method for calculating the approximate position of the knee in multiple dimensions, when multiple loads are acting on it [26]. RBFs provide a means for making approximations from multivariate data sets based on the distance the point to approximate is from the experimental data. RBFs have been

used in the past to describe data sets with high dimensionality, and can reliably describe data sets with a scattered or unknown distribution [24,25].

The introduction of RBFs to calculate the total constraint of the passive knee joint has allowed for a unified envelope (UE) description of the knee to be identified, with a continuous relationship between the dependent (applied loads and flexion angles) and independent (positions) variables [35]. Using RBFs to approximate the multidimensional load-displacement response of the knee makes comparisons between knees much easier, because RBFs allow for the approximation of multidimensional loading configurations to be calculated for any knee, without the need to collect data around that specific loading configuration. The UE can be calculated across a common grid space of applied loads and flexion angles, allowing for the comparison of many different loading configurations at once.

Unfortunately, the UE will only provide a single estimate for the position of the knee at any given combination of loads and flexion angle, without a measure of how confident it is in that estimate. This means that the current methods for using RBFs to describe the UE assumes that a given loading condition has a single position, regardless of the loading path taken to get there. In other words, RBFs can help calculate a multidimensional surface of best fit, but the accuracy of this surface isn't clear [27].

The primary objective of this study was to develop a measure of uncertainty in the calculated UE without sacrificing any of the benefits that have been associated with using RBFs to describe the data. There are also two secondary objectives in this study, the first is to make the UE more robust to changing investigators. A decrease in the difference between two investigator's UEs on the same knee should increase confidence in the ability of both UEs to describe the knee in question. The last objective is to determine the best protocol for loading

when collecting data, specifically whether multiaxial loading is necessary to collect, or if uniaxial loading alone is able to adequately describe the knee.

3.3 Methods

Experimental data were collected on one fresh-frozen cadaveric leg (Male, Age: 67 years, BMI: 19). The specimen was thawed for 24 hours before tissue farther than approximately 20 cm from the epicondylar axis (both proximal and distal) was removed to allow for cylindrical aluminum fixtures to be attached with bone cement to both the femur and tibia. The fibula was secured to the tibial fixture to prevent any relative motion. The femoral fixture was mounted in an inverted-vertical position (Fig. 1) while the tibial fixture was attached to a 6-DOF tri-axial load cell (JR3 Inc., USA) and an analog foot. Both the femoral and tibial fixtures had rigid body markers attached to them, and positions were tracked using an Optotrak Certus infrared camera system (NDI, Canada). Both loads and kinematics were collected at 100Hz. After the laxity evaluations were performed, the specimen was dissected down further to identify and digitize bony landmarks on both the femur and tibia. These points were used to set up the coordinate system to calculate relative motion between the tibia and femur based on Grood and Suntay's 3-cylindrical open-chain coordinate system [17].

The specimen then underwent a full laxity evaluation. A full laxity evaluation involves manually applying a range of loads to the distal end of the tibia in one primary DOF at a time (uniaxial loading) throughout the full flexion range of the specimen. The three primary loads and torques were varus-valgus torque (VV) (± 16 Nm), internal-external torque (IE) (± 6 Nm), and anterior-posterior force (AP) (± 60 N), and they were applied by smoothly alternating between

positive and negative loads and torques at different flexion angles. Along with the three uniaxial loading conditions, multiaxial loading evaluations were also performed with loading applied in two of the three axes at a time. Full laxity evaluations were performed by three different investigators, each with a different level of experience performing laxity evaluations ranging from very experienced to a first-time investigator, to determine the effect of investigator and experience level on the final UE. The first investigator performed their laxity evaluation for approximately three times as long as the others to determine if the collection of more data resulted in a meaningful change to the UE. All three laxity evaluations were performed within 2 hours of each other to minimize the effect of tissue degradation. Each evaluation was assisted by a near real-time LabVIEW interface that gave visual feedback for the applied loading at different flexion angles (Fig. 2). This helped ensure that applied loading was consistent and that experimental data were collected across all desired conditions by all investigators.

After data collection, the kinematics and loads were transformed into the Grood and Suntay coordinate system for analysis. Then data from the load cell were used to separate the experimental data into loading and unloading portions. Data that were collected while the overall applied load was increasing was retained, while data collected while the overall applied load was decreasing were removed. The loading data were then used as training data to develop multiple radial basis functions (RBF) for each investigator's laxity evaluation.

For this study, four independent variables [knee flexion angle ($^{\circ}$), VV torque (Nm), IE torque (Nm), and AP force (N)] were used to solve for three dependent variables [VV angle ($^{\circ}$), IE angle ($^{\circ}$), and AP position (mm)] (Fig. 3). The three loads were scaled by 95% of their range along with flexion angle, which was also scaled by 95% of its range, to get all variables on approximately the same scale. In this study, RBFs were applied in two steps of the analysis.

First, in order to determine how well RBFs can approximate known data, they were trained with some of the experimental data withheld and then used to predict that withheld data. Then RBFs were used to calculate the UE with three dependent variables across a generic, evenly spaced grid of independent variables to allow for comparisons between knees.

First, in order to estimate how well RBFs can approximate known positions of the knee, each individual loading path was removed from the data set, and then approximated using an RBF trained with the remaining data. Kinematics of the knee depend on the forces applied to it, but also on the previous position the knee was in. In other words, observed positions of the knee are both load and path dependent. Therefore, in order to determine how well RBFs are able to predict observed data, random data removal is not ideal because the RBF can use nearby points along each loading path to reliably interpolate the randomly removed points. However, each loading path, when treated as a whole, is independent from every other loading path. By removing one full path from the data set and using an RBF fit to all other paths to predict it, it is possible to see how well the RBF can predict independent points, like the grid points of the UE. The number of loading paths for each investigator and loading type is shown in Table 1, along with the total number of data points collected.

Once a path was removed, the remaining data were sequentially downsampled (SDS) by taking every fifth data point collected starting at the first data point, then the second, third, fourth, and finally fifth data point. This results in five nearly equal data sets that can be used to train five different RBFs, which can then be used to get five slightly different predictions for each point along the removed path (Fig. 4). The data were downsampled because otherwise, the RBF puts too much weight into the closest group of points, creating a UE that is locally overfitting to the data, rather than picking up on the broader patterns of the knee. After the five

RBFs were used to get five predictions, the same downsampling, training, and prediction process was repeated 10 times using every 10th point, 20 times using every 20th point, and 40 times using every 40th point to get a total of four downsampling cases with a total of 75 different predictions ($5 + 10 + 20 + 40 = 75$) for each point along the path (Fig. 4). The RBF is robust to this kind of downsampling because, based on the cumulative power spectrum density, over 99% of the power in both the input and output signals are contained in frequencies less than 2.5Hz (every 40th point of 100Hz signal) (Fig. 5) and RBFs have been shown to approximate the UE well with fewer than 900 well-spaced points [26].

The mean and variance of the predictions from each of the four downsampling cases were calculated (i.e. the mean and variance of the results from the 5 RBFs trained with every 5th point, 10 RBFs trained with every 10th point, 20 RBFs trained with every 20th point, and 40 RBFs trained with every 40th point) and then an overall mean and variance were found (Fig. 4) by weighting each of the four downsampling cases equally, rather than weighting each of the 75 predictions equally (this gives more weight to the results from the RBFs that were trained with more data). This gave a single prediction for every point, along with the variance for that prediction. Unfortunately, the variance from just the RBFs predictions was too small to accurately describe the observed uncertainty. To correct for this, the mean variance of each dependent variable (VV angle, IE angle, AP position) was compared to the variance seen in the difference between the observed data and predicted points for that dependent variable. This gave a variance difference for each dependent variable that, when added to the variance calculated from the RBFs, uniformly shifted each prediction's variance up to more closely match the observed variance (Table 2). This shift is also used to increase the variance for each dependent variable in the generic UE.

RBFs were also used to calculate the UE across a generic grid of evenly spaced independent variables, rather than observed independent variables, to allow for comparisons between knees and investigators. The grid was designed to stay within the range of experimentally collected data, and included 13 flexion angles (every 10° from 0° to 120°), 17 VV torques (every 2 Nm from -16 Nm to 16 Nm), 13 IE torques (every 1 Nm from -6 Nm to 6 Nm), and 13 AP forces (every 10 N from -60 N to 60 N) to give 37,349 evenly spaced points. The same sequential downsampling process used to predict points along loading paths was also used here to calculate 75 different UEs. The means and variances of each downsampling case were found and used to find an overall mean and variance for the SDS-UE (SDS will be used to differentiate when the UE is calculated using the method proposed in this paper, rather than the previous method), in the same way an overall mean and variance were found earlier when predicting paths. The final step was to increase the variance for each dependent variable throughout the SDS-UE by the variance shift that was used to fit predicted data to observed data.

Each of the three investigator's laxity evaluation data were kept separate through every step and were used to calculate four different UEs used for data analysis. The first UE was calculated using the previous method for each investigator. This was to identify the differences between the previous method for calculating the UE and the method proposed in this paper, or the SDS-UE. Along with the main SDS-UE for each investigator, calculated with all available loading data collected by an individual investigator, two other SDS-UEs were calculated, giving a total of 9 SDS-UEs and 3 UEs from the previous method. One SDS-UE was trained with only the uniaxial loading trials and the other was trained with only multiaxial loading trials. By using each SDS-UE's overall mean and shifted variance, it was possible to directly compare

differences between knee envelopes and comment on whether or not the difference was significant.

3.4 Results

3.4.1 Visualizing the UE in 3D

To visualize the UE, isosurface renderings of the first investigator's SDS-UE were created from 0° to 120° flexion (Fig. 6) at 50% and 100% of the largest magnitude of calculated IE and VV torques, normalized to their respective maximums (16 Nm of VV torque and 6 Nm of IE torque). As the flexion angle increases the plot appears to become wider along both the VV and IE axes. This means the knee has a larger range of motion at 120° flexion than it does at 0° flexion for both IE and VV motion. Notice that the UE is showing a pure external load along the top spine of the plot. This top spine is the motion of the knee at 100% of the applied IE torque (6 Nm) and 0% of the applied VV torque while the bottom spine is the motion at 100% of the IE torque applied internally (-6 Nm). Similarly, the top and bottom spine of the red isosurface is the motion of the knee at 50% IE torque (3 Nm). When the data with a valgus load is omitted (Fig. 6C), these spines are represented more clearly as the edges of the UE at 50% and 100% IE torque. The left and right spines of the UE should be thought of in the same way, but with an applied VV torque rather than IE torque (Fig. 6B).

3.4.2 Uniaxial Loading vs Multiaxial Loading

Along with the main SDS-UE, found by training the RBF with all the loading trials collected by a single investigator, two other SDS-UEs were calculated. One was calculated using only the uniaxial loading trials, and the other with only the multiaxial loading trials. To visualize how the SDS-UE changes when different loading data is used, Figure 7 has these two cases plotted together for investigator 1. The center column of plots show the UE with only one torque applied at 5 magnitudes [100% (top line), 50%, 0% (center line), -50%, and -100% (bottom line)] in the direction of each plot's Y-axis (i.e. lines in top row of plots show different VV torques while lines in the bottom row show different IE torques) while the outside plots show the UE at $\pm 100\%$ IE (top row) or VV (bottom row) torque with the same 5 load magnitudes. The top center plot in Figure 7 should be thought of as a top view of the edges in plot B of Figure 6 with an extra line at 0 Nm of applied torque, while the bottom center plot in Figure 7 should be thought of as a side view of the edges in plot C of Figure 6. Notice that the uniaxial and multiaxial UEs perform very similarly when looking at only one applied torque at a time (center column of plots and middle lines of outside plots), but there are large differences whenever multiaxial loading is applied.

To numerically compare each type of loading, Table 3 shows the median absolute difference (MAD) between all investigators for each variable and type of loading, along with the percent of grid points that are significantly different (two-tailed t-test, $p < 0.05$) for each variable between. Note that Table 3 is comparing all investigators, so the values shown are the averages from all investigator comparisons (I1 vs I2, I1 vs I3, and I2 vs I3). There is a decrease in average MAD for all variables when comparing SDS-UEs trained with only uniaxial loading data to

SDS-UEs trained with only multiaxial loads, and another decrease when the SDS-UEs have access to both types of loading data for training. The trend for significant differences (two-tailed t-test, $p < 0.05$) between investigators is similar with almost all variables showing a decrease in significant differences from only uniaxial loading to only multiaxial loading, and again from only multiaxial loading to both types of loading.

3.4.3 Comparing investigators and methods

The median absolute difference was calculated between each investigator's UE using both the previous method and SDS method at all grid points in the UE (Table 4). A lower median absolute difference suggests the UEs are more similar to each other, and that the method for calculating the UE is less dependent on who the investigator is. On average, the MAD decreased by 18.3% in VV angle difference, 15.6% in IE angle difference, and 16.2% in AP position with the SDS method. The largest MAD between UEs is found when comparing investigator 1 to investigator 3 for all variables and both methods.

To visualize the differences between methods, Figure 8 shows the range of all investigators UEs when calculated using both the previous method (red) and the SDS method (blue). It is clear from the figure that the SDS method produces much smoother lines, this is most noticeable at the 0 Nm IE and 0 Nm VV lines where the previous method shows sharp points, rather than gradual changes. The previous method also has a larger range between investigators than the SDS method at nearly every torque and flexion angle, leading to only a few places where the range of the SDS method isn't already covered by the range of the previous method.

3.4.4 Standard Deviation and Significant Differences

As a result of the way variance is uniformly shifted, the SDS method for estimating the standard deviation of the UE produced values that are skewed to the right, or positively skewed, for all variables and investigators (Table 5). It also produced standard deviations that are investigator dependent, sometimes leading to little overlap in the range of standard deviation. For example, the minimum standard deviation found for the VV angle of investigator 2 is 0.33° while the maximum for investigator 3 is 0.36° . These factors make comparisons between absolute standard deviation difficult, but by making comparisons with the percentile of standard deviation, regions of more or less certainty become clearer.

By averaging the percentile of standard deviation found for each variable and investigator, relative comparisons of overall uncertainty can be made. Figure 9 shows the 100% load magnitude surface of the average SDS-UE from all investigators, colored by the average quartile of standard deviation for all variables [VV ($^{\circ}$), IE ($^{\circ}$), and AP (mm)] and investigators (I1, I2, and I3) in that region. The colors should be interpreted as regions of higher (red) and lower (blue) relative uncertainty in the ability of the RBF to approximate the SDS-UE. The areas of above average standard deviation (colored yellow for the 50th to 75th percentile, and red for anything above the 75th percentile) are concentrated near 0° and 120° flexion, and areas where both IE and VV torques are being applied (multiaxial loading). The lowest standard deviations appear near the four spines of the SDS-UE (i.e. areas of either maximum or minimum VV or IE angles). Generally, these are the areas where only one torque is acting on the knee (uniaxial loading).

The benefits of using the SDS method to calculate the UE over the previous method are best on display in Figures 9 and 10. Both figures are comparing investigator 1's UE to investigator 2's UE, but Figure 10 is colored by VV° difference while Figure 11 is comparing IE° . The first plot, A, in both figures was made using the previous method for calculating the UE. In both figures, plot A shows the largest differences and the most area with differences. Plot B and C were created using only the SDS method and had only significant differences colored (one-tailed t-test). In plot B the significance level was set at $p < 0.2$ while plot C had $p < 0.05$. Plot C should be thought of as the better comparison for both figures, showing almost no significant differences in either figure. Plot B in both figures demonstrates how the SDS-UE performs in areas where the previous method showed the largest differences. Figure 10 shows the previous method had a large area of difference, from roughly the 20° to 70° flexion range, of about $0.6^\circ VV$. The same place in plot B has a much smaller area, and the difference decreased to around $0.4^\circ VV$. Figure 11 has an area in about the same place that shows a difference of up to $-6^\circ IE$ when using the previous method. In plot B, the same place has a difference of less than half the magnitude of plot A, over much less area. Overall, the SDS method shows smaller differences between investigators and produces easier to interpret plots.

3.5 Discussion

The results from this study suggest that the SDS method is less dependent on the investigator collecting the data, while providing a method for estimating whether observed differences between knees were significant, based on the uncertainty in the RBF predictions. The data show less variation investigator-to-investigator with the SDS method for each dependent

variable. The SDS method also provides a smoother, more continuous relationship between independent (loads and flexion angle) and dependent variables (positions) than the previous method. These factors all point to the SDS method producing more consistent and accurate UEs than the previous method.

The main goal of this paper, however, was not to improve accuracy or consistency of the UE, but rather to determine how well the calculated UE describes the knee in question, and which conditions cause an increase or decrease in the uncertainty of the predicted position of the knee. To summarize how this was accomplished, it was first determined how well the RBF could predict real-world data. This information was used to calculate an average observed variance for RBF approximations, which was compared to the variance of the RBF predictions from the decimation cases. The difference in these variances, called the variance shift, was used to uniformly shift up the variance for the grid points in the SDS-UE. This method resulted in the heavy right skew in the distribution of standard deviations. It also means that there is a minimum standard deviation for each variable that is determined by the variance shift calculation. For example, if all 75 RBF predictions for a single point were the exact same, then the variance of the RBFs prediction would be 0, so the standard deviation at that point would simply be the square root of the variance shift. This method appears to perform well by limiting areas of overconfidence with the variance shift, while also allowing for larger standard deviations where appropriate, such as regions of high flexion or multiaxial loading.

The final objective of this paper was to determine the best protocol for evaluating laxity during data collection. It was found that SDS-UEs calculated with only uniaxial loading data had the largest MAD between investigators for all variables, along with the most significant differences. There was a large improvement when using only multiaxial loading data, likely

because the majority of the grid points for the UE have multiaxial loading, but using all loading data was the most consistent. The difference in the total amount of data collected appeared to have little effect on the final envelope. Investigator 2 and 3 each collected approximately 10 minutes of laxity evaluations, and their final envelopes were very similar to Investigator 1, who collected closer to 30 minutes of data. The viscoelastic properties of the ligaments in the knee can influence measurements of laxity, with studies showing a decrease in ACL stress by 50% over 2 hours of constant strain [36]. However, stress relaxation is slower during cyclic loading and the time scales used in this study make it unlikely that the speed of loading path had a meaningful effect on the final envelope with investigator 1 having an average path length of 0.77 seconds, 0.60 seconds for investigator 2, and 1.01 seconds for investigator 3. Therefore, the most important aspect of data collection is collecting both kinds of loading data for approximately 10 minutes total, with the speed of loading path likely having a relatively minor effect.

To determine if an investigator's previous experience performing laxity evaluations had an effect, each investigator in this study had a different level of experience. Investigator 1 had the most experience performing laxity evaluations and felt comfortable with no instruction needed, investigator 2 had limited experience and required some instruction, and investigator 3 had no prior experience. It is difficult to determine exactly how much of a factor experience was, but the largest MAD was found between investigators 1 and 3. However, this difference could have been influenced by the amount of time the knee had been sitting out, investigator 1 performed the first laxity evaluation, followed by investigator 2, and last was investigator 3. Regardless of how much experience makes a difference, the SDS method produced more consistent UEs, which reduces the need for experience relative to the previous method.

This method can benefit a variety of future work involving the passive envelope of constraint in the knee. It allows for more consistent envelopes between investigators, reducing the need to control for investigator. This method can theoretically be applied to ligament testing, helping to identify regions in the UE with more or less confidence in observed differences. The UE has been used in the past to identify changes in constraint due to full ligament tears [37], but due to the increased robustness it may now be able to reliably pick up on smaller changes in constraint, perhaps from partial ligament tears or meniscal injuries. It can also be applied when researching total knee replacements, helping to identify how different components can constrain movement relative to both the natural knee and to other knee replacement components.

In conclusion, the method presented in this paper for calculating UEs has been shown to be more consistent between investigators, and more useful when comparing different UEs. It can be applied to a wide range of topics involving knee laxity and what contributes to the constraints of the knee in multiple DOFs. There are also likely to be applications in measuring and comparing the constraint of other joints, for example when comparing hip replacements to the natural hip, or to other hip replacement options. Applications could also be found in other work involving quantifying uncertainty, or specifically in quantifying uncertainty from RBFs. Overall, this method helps to create a more complete understanding of the passive knee envelope and how different degrees of freedom in the knee are related.

3.6 Tables

Table 1: Number of paths and data points by each investigator and loading type

Investigator	Uniaxial Loading	Multiaxial Loading	Total
1	298 paths 20,972 points	767 paths 61,471 points	1,069 paths 82,694 points
2	197 paths 10,210 points	233 paths 15,710 points	431 paths 25,942 points
3	106 paths 10,957 points	145 paths 14,395 points	251 paths 25,317 points

Table 2: Values for the calculated variance from the RBFs, the observed variance from the difference between predicted and measured values, and the difference between the two used to uniformly shift the variance from the RBFs up to match the observed variance.

	Varus-Valgus (°)			Internal-External (°)			Anterior-Posterior (mm)		
	RBF	Observed	Shift	RBF	Observed	Shift	RBF	Observed	Shift
I1	0.009	0.07	0.06	0.15	1.08	0.93	0.02	0.11	0.09
I2	0.013	0.12	0.11	0.26	2.06	1.80	0.03	0.26	0.23
I3	0.005	0.07	0.07	0.06	0.91	0.84	0.02	0.22	0.20

Table 3: Average MAD of SDS-UEs and average percent of the SDS-UE that is significantly different (two-tailed t-test, $p < 0.05$) between investigators separated by dependent variable and type of loading used to train RBF.

	Average MAD			% Significantly Different		
	Uniaxial	Multiaxial	Both	Uniaxial	Multiaxial	Both
VV (°)	0.32	0.29	0.24	17.9%	7.6%	6.3%
IE (°)	1.05	0.81	0.72	18.4%	3.5%	3.7%
AP (mm)	0.99	0.48	0.39	36.7%	10.0%	9.0%

Table 4: Median absolute difference of UEs between investigators at every grid point of the UE when using both the previous method and the SDS Method along with the relative percent decrease in median absolute difference from the previous method to the SDS method.

	Median Absolute Difference						Relative Decrease in Median Absolute Difference		
	Previous Method			SDS Method			VV (°)	IE (°)	AP (mm)
	VV (°)	IE (°)	AP (mm)	VV (°)	IE (°)	AP (mm)			
I1 vs I2	0.25	0.85	0.36	0.20	0.66	0.31	21.7%	22.4%	12.0%
I1 vs I3	0.35	0.97	0.57	0.30	0.80	0.50	14.6%	17.0%	13.4%
I2 vs I3	0.29	0.75	0.48	0.23	0.70	0.37	19.8%	6.1%	22.6%
Average	0.30	0.86	0.47	0.24	0.72	0.39	18.3%	15.6%	16.2%

Table 5: Minimum (0th Percentile), median (50th Percentile), and maximum (100th Percentile) values for standard deviation for each investigator and output.

	Varus-Valgus (°)			Internal-External (°)			Anterior-Posterior (mm)		
	Min	Median	Max	Min	Median	Max	Min	Median	Max
I1	0.24	0.25	0.56	0.97	1.00	1.95	0.31	0.32	0.62
I2	0.33	0.34	0.58	1.34	1.37	2.57	0.48	0.50	0.98
I3	0.26	0.27	0.36	0.92	0.93	1.47	0.45	0.46	0.74

3.7 Figures

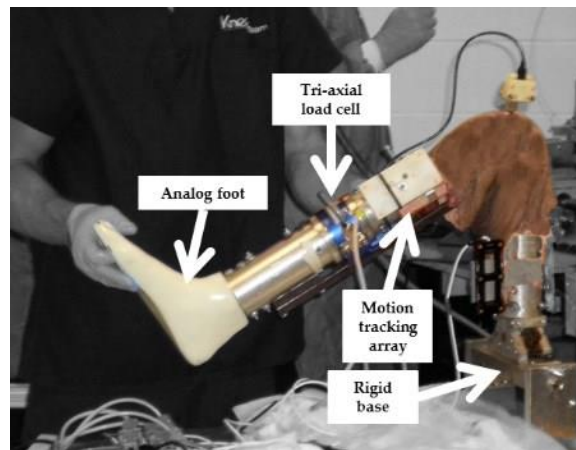


Figure 1: Manual laxity evaluation setup [35]

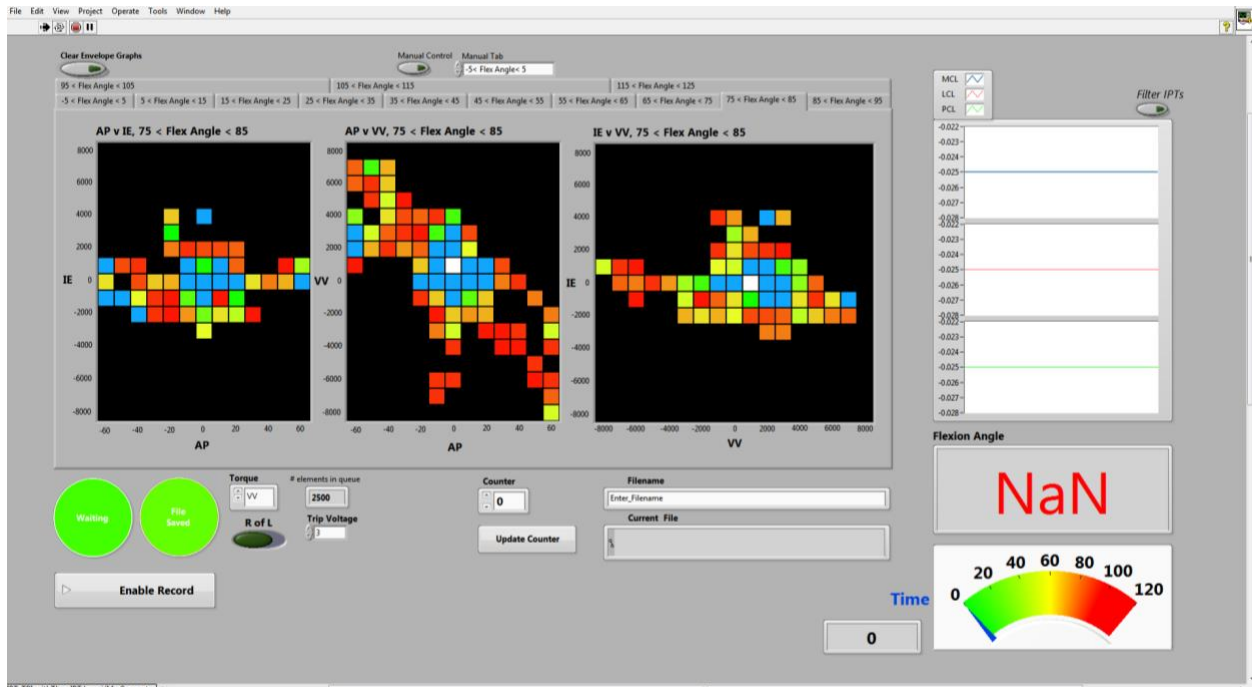


Figure 2: LabVIEW Interface providing near real-time feedback for laxity evaluations. Square color would change as more data were collected within each square, black means no data has been collected in that region.

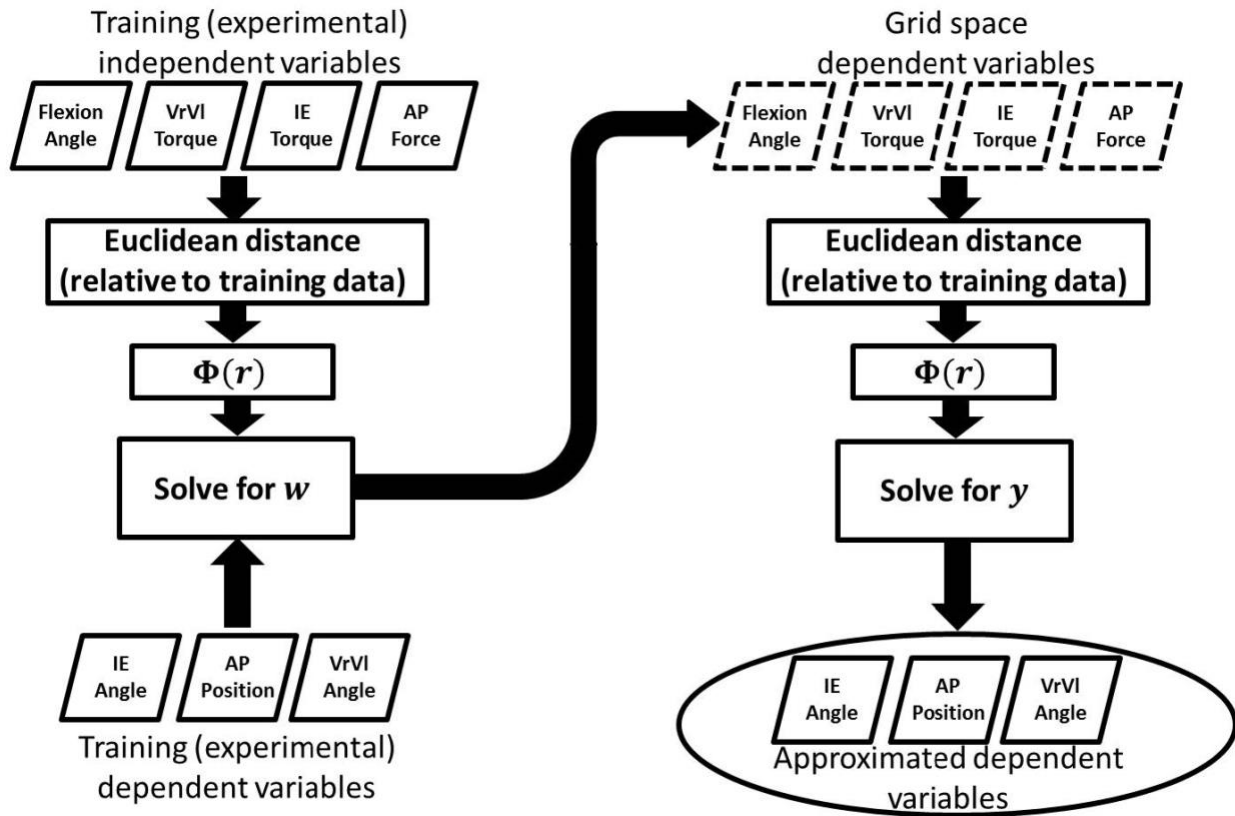


Figure 3: RBF flowchart. Experimental data is used to determine the weight of each experimental point, then the weights are used to estimate dependent variables through a generic, evenly spaced grid [26].

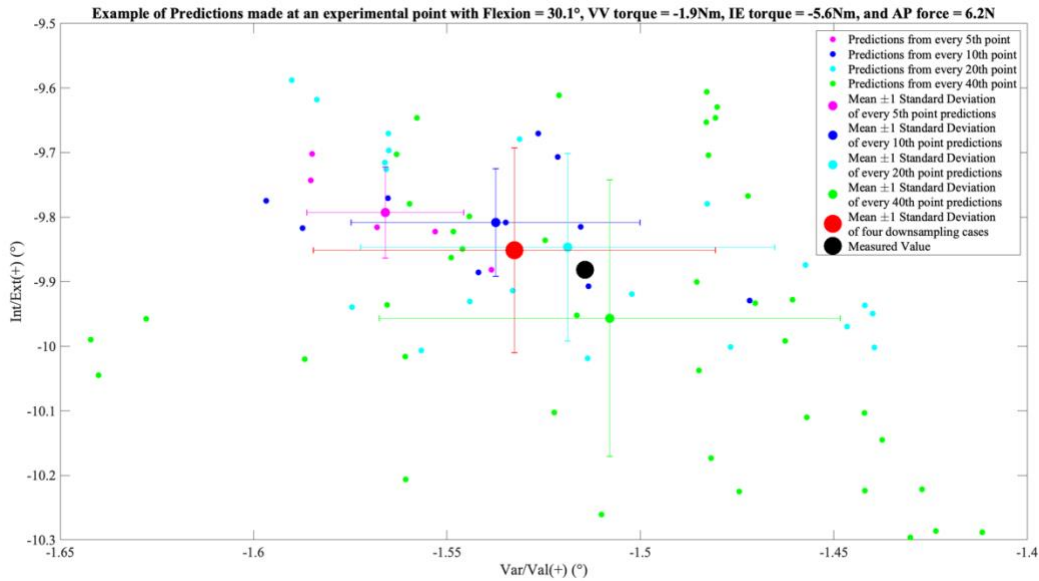


Figure 4: Example of predictions made for one experimental point at 30.1° Flexion, -1.9Nm VV torque, -5.6Nm IE torque, and 6.2N AP force. All four downsampling cases are included with the 5 predictions made from every 5th point in magenta, 10 predictions from every 10th point in blue, 20 predictions from every 20th point in cyan, and 40 predictions from every 40th point in green. Included are the four means ± 1 standard deviation of each downsampling case. The red dot is the mean of the four downsampling case means ± 1 standard deviation and the black dot is the measured value that was being predicted.

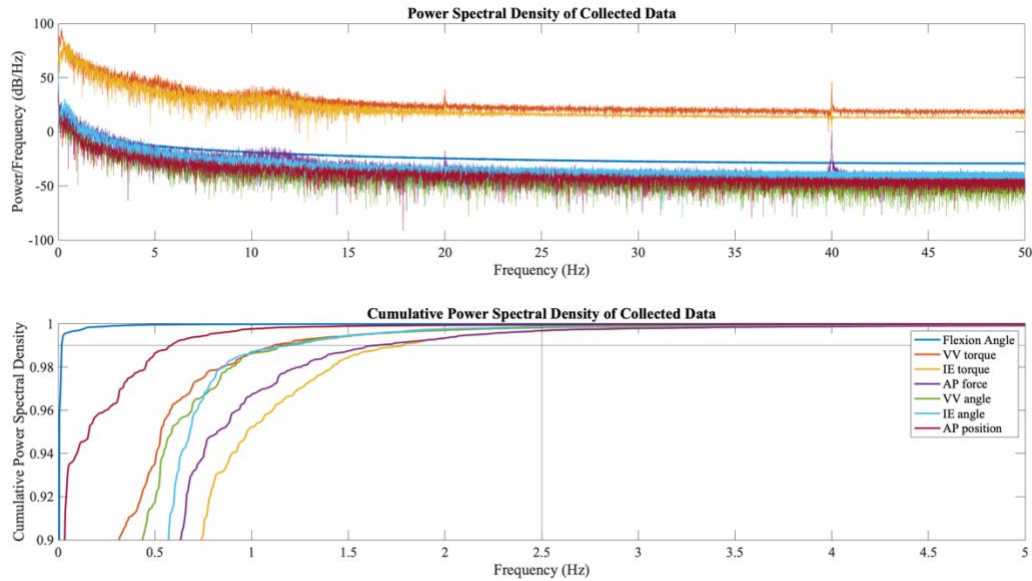


Figure 5: Power spectral density and cumulative power spectral density for one laxity evaluation trial with VV torque and IE torque applied by investigator 1. Cumulative power spectral density chart is showing cumulative power from 0.9 to 1 and frequency from 0 to 5 Hz to help differentiate between variables. Two other lines are included, one horizontal line at 99% cumulative power and one vertical line at a frequency of 2.5 Hz, to show that over 99% of the power in all signals are contained in frequencies below 2.5 Hz (every 40th point from a 100Hz signal).

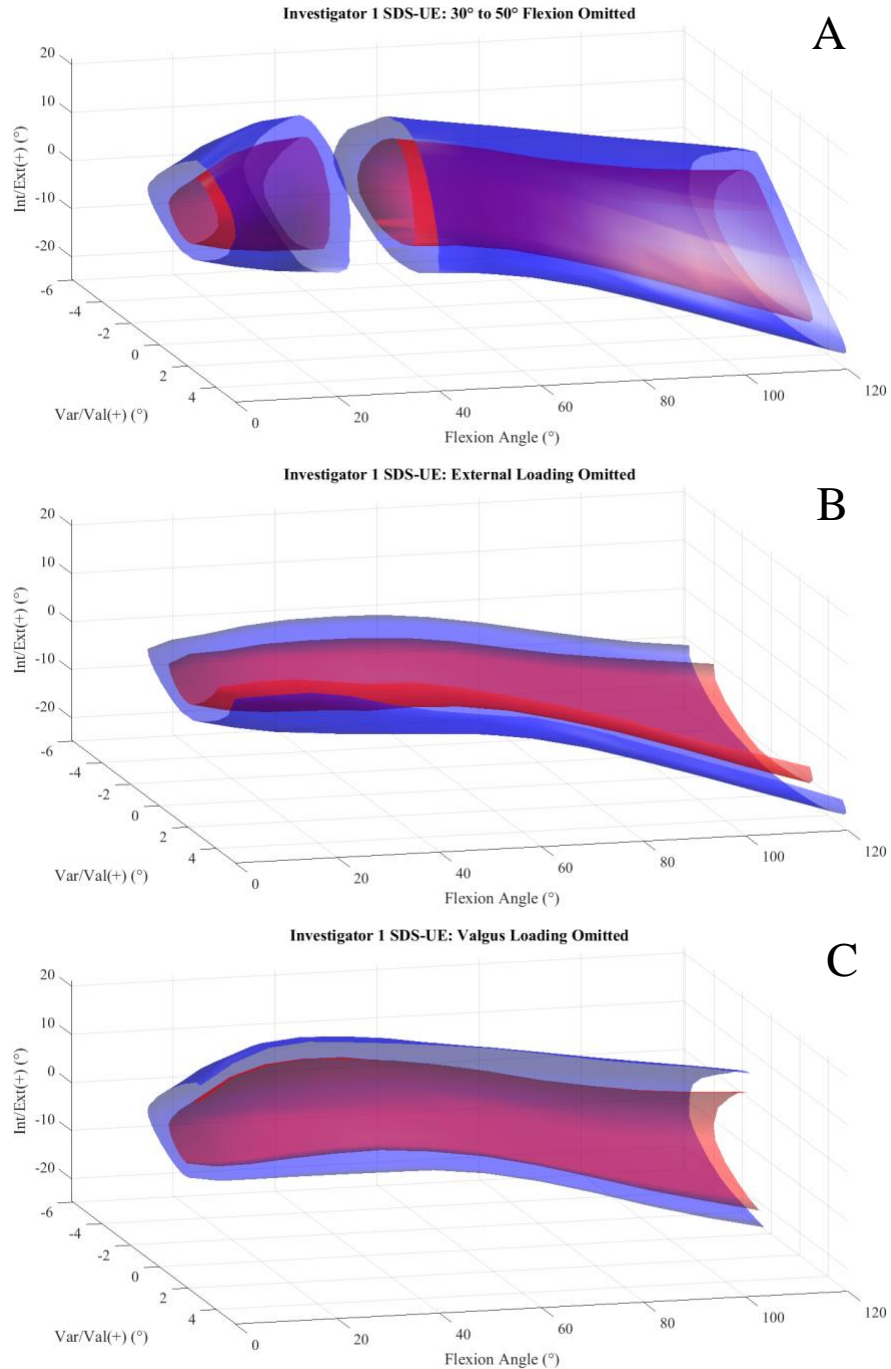


Figure 6: Investigator 1’s UE calculated using the SDS method represented by isosurface renderings at constant load magnitudes, scaled by their respective maximums (16 Nm of VV torque and 6 Nm of IE torque). The blue surface is at 100% magnitude and the red surface is at 50%. **A:** Data between 30° and 50° flexion is omitted for visualization. **B:** Data with an external load is omitted for visualization. **C:** Data with a Valgus load is omitted for visualization.

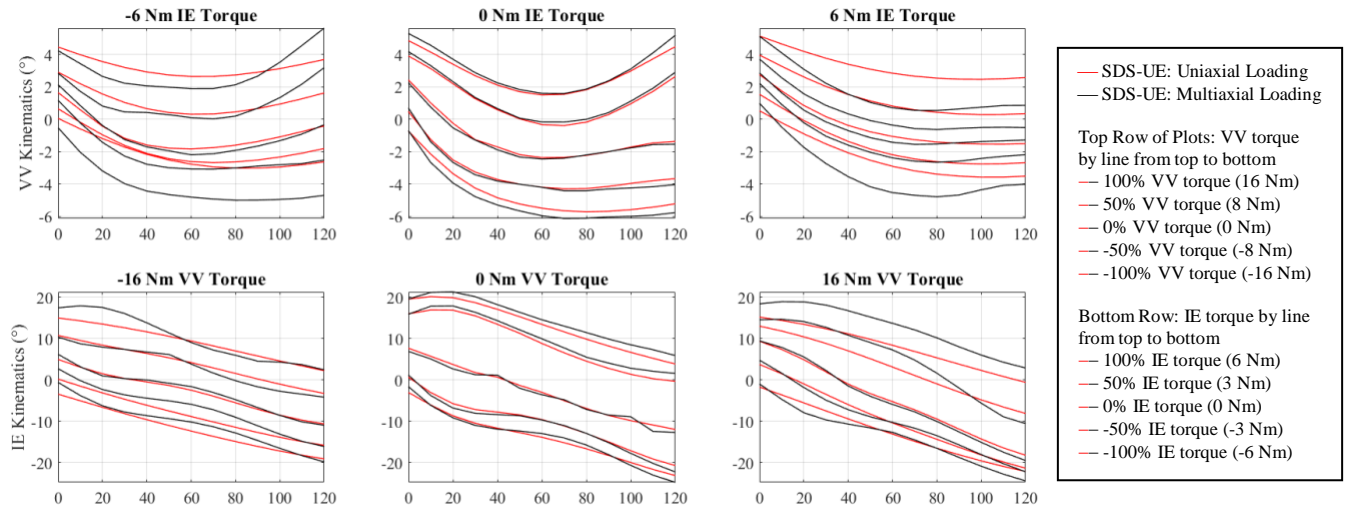


Figure 7: Investigator 1's SDS-UE trained with only uniaxial loading trials shown in red, and trained with only multiaxial loading trials shown in black. Top row has VV kinematics vs flexion angle at -100% (left), 0% (center), and 100% (right) applied IE torque (-6 Nm, 0 Nm, 6 Nm). The lines in the top row correspond to applied VV torques at -100% (bottom line, -16 Nm), -50%, 0% (center line, 0 Nm), 50%, and 100% (top line, 16 Nm). Bottom row shows IE kinematics vs flexion angle at -100% (left), 0% (center), and 100% (right) applied VV torque (-16 Nm, 0 Nm, 16 Nm). The lines in the bottom row correspond to applied IE torques at -100% (bottom line, -6 Nm), -50%, 0% (center line, 0 Nm), 50%, and 100% (top line, 6 Nm).

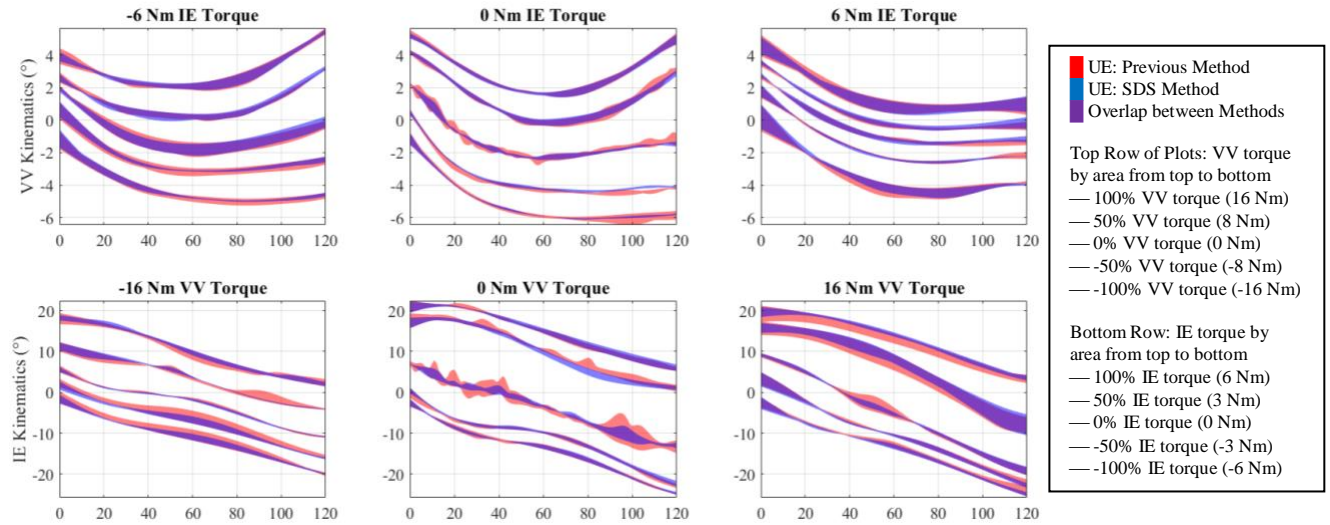


Figure 8: Range of all Investigators UEs calculated with the previous method shown in red and the SDS method in blue, areas with overlap are colored purple. Top row has VV kinematics vs flexion angle at -100% (left), 0% (center), and 100% (right) applied IE torque (-6 Nm, 0 Nm, 6 Nm). The lines in the top row correspond to applied VV torques at -100% (bottom line, -16 Nm), -50%, 0% (center line, 0 Nm), 50%, and 100% (top line, 16 Nm). Bottom row shows IE kinematics vs flexion angle at -100% (left), 0% (center), and 100% (right) applied VV torque (-16 Nm, 0 Nm, 16 Nm). The lines in the bottom row correspond to applied IE torques at -100% (bottom line, -6 Nm), -50%, 0% (center line, 0 Nm), 50%, and 100% (top line, 6 Nm).

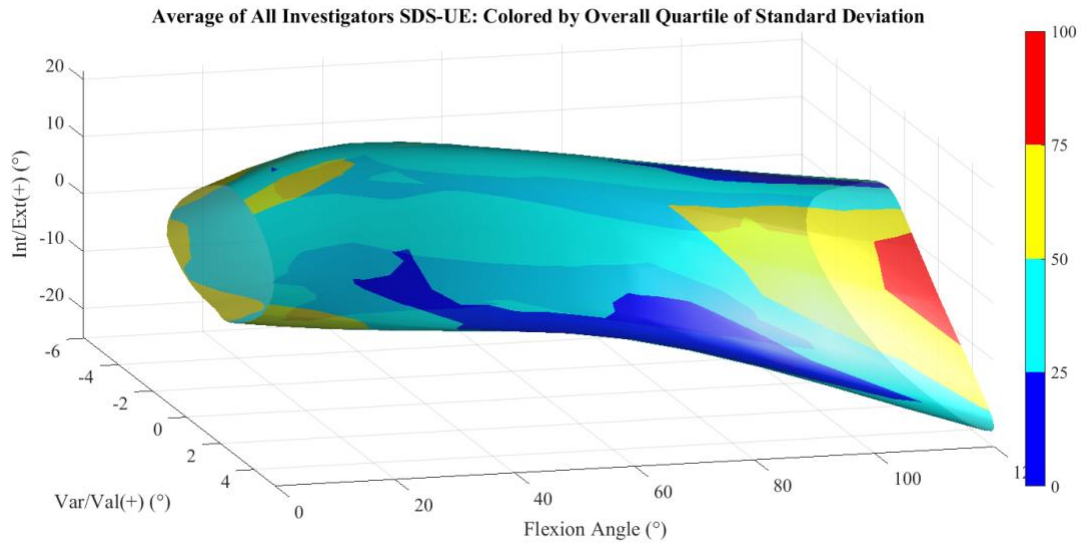


Figure 9: Average of all investigators SDS-UE at 100% load magnitude colored by overall standard deviation quartile of all variables and investigators (i.e. the percentile of VV standard deviation, IE standard deviation, and AP standard deviation for I1, I2, and I3 was found at each grid point of the SDS-UE. The overall standard deviation quartile was found by averaging these nine standard deviation percentiles).

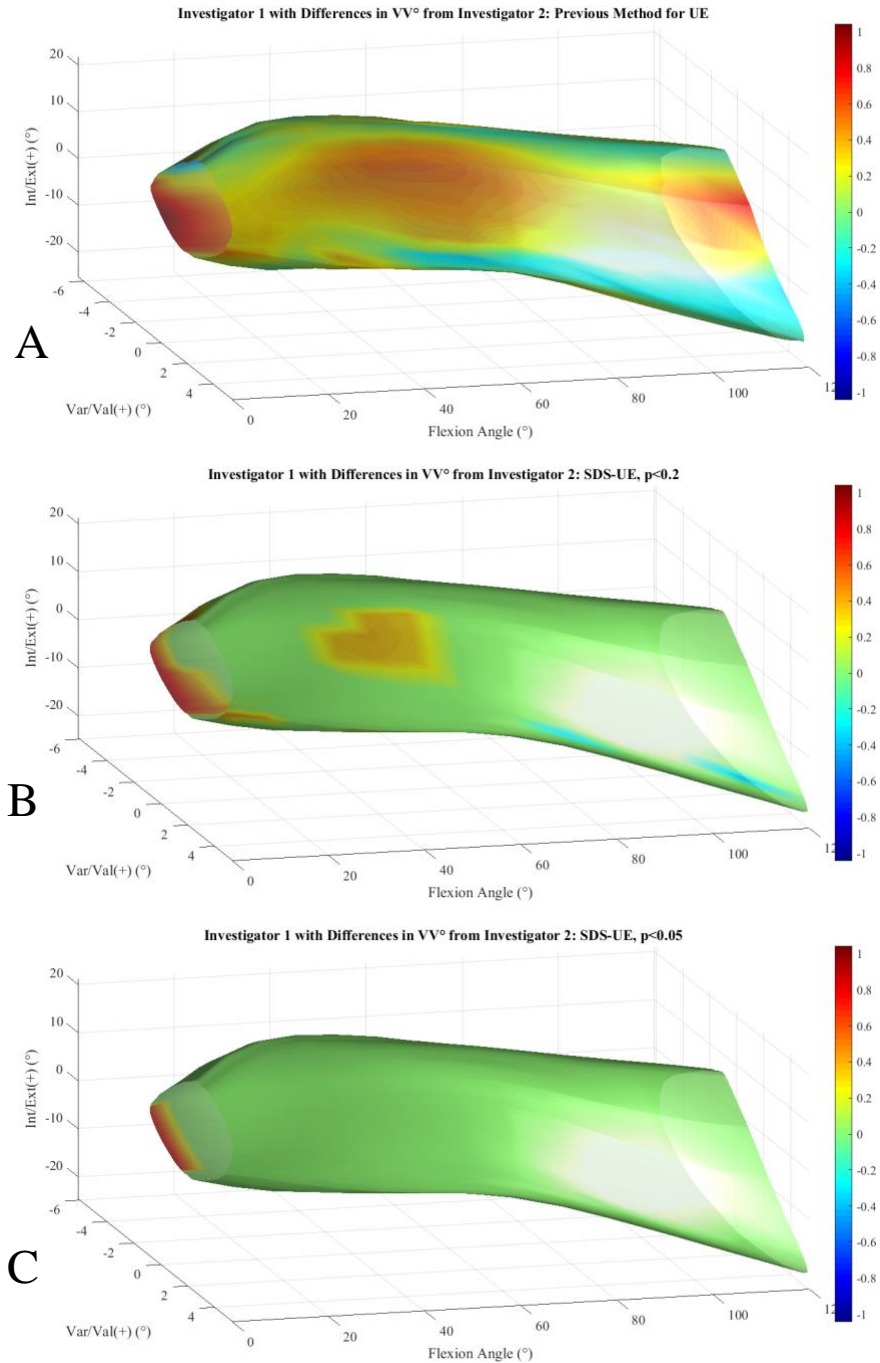


Figure 10: Investigator 1's UE at 100% load magnitude colored by how much it differs in VV° from Investigator 2's UE at 100% load magnitude. **A:** Previous method for the UE was used for the plot and in the difference calculation for color. **B:** SDS method for the UE was used for the plot, in the difference calculation, and to determine significance. Only significant differences are colored (one-tailed t-test, $p < 0.2$). **C:** Same as plot B with $p < 0.05$ rather than $p < 0.2$.

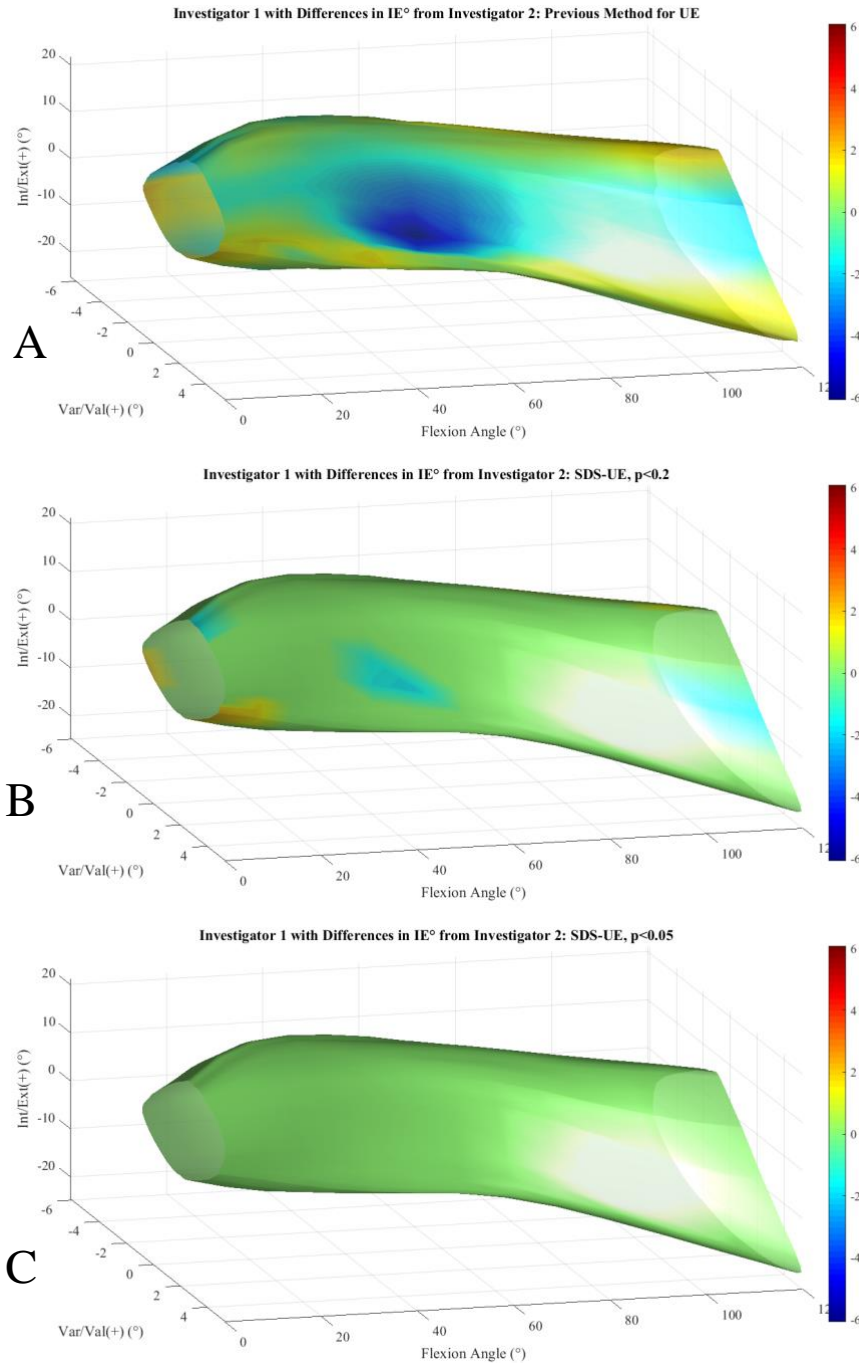


Figure 11: Investigator 1’s UE at 100% load magnitude colored by how much it differs in IE° from Investigator 2’s UE at 100% load magnitude. **A:** Previous method for the UE was used for the plot and in the difference calculation for color. **B:** SDS method for the UE was used for the plot, in the difference calculation, and to determine significance. Only significant differences are colored (one-tailed t-test, $p < 0.2$). **C:** Same as plot B with $p < 0.05$ rather than $p < 0.2$.

Chapter 4: Conclusion

The primary objective of this thesis was to incorporate a measure of uncertainty into the UE. This measure could ideally be applied to any comparison between UEs, and allow for comments on the significance of observed differences, rather than only reporting on the magnitude of observed differences. This measure needed to be created in a way that didn't sacrifice any of the previously reported benefits of using RBFs to describe the UE, and would ideally show improvements in objective measures. Therefore, the secondary objectives were to reduce the difference seen between investigators and to determine the optimal protocol for laxity evaluation.

The introduction of the sequential downsampling method in chapter 3 provided the means for all objectives to be met. The variance estimate was created in a two-step process that utilized sequential downsampling in both steps. First, there was the specific variance, calculated at each grid point of the UE and for each variable. This was based on how much variation was seen in the UEs trained with different sets of sequentially downsampled data. Second, there was a general variance, determined by how well the RBFs could predict known data that was withheld from training. These two values were combined to provide a standard deviation that was specific to each knee, investigator, and variable, while also matching what has been observed by previous studies [38].

Improvements related to the secondary objectives were also found. On average, the median absolute difference between investigators has been reduced by 18.3% in VV° , 15.6% in IE° , and 16.2% in AP position. This reduces the effect the researcher has on the UE and reduces the dependence on experience, which lowers the barrier to entry for other labs to start performing

this kind of analysis. This research also verified the importance of collecting laxity evaluations with both uniaxial and multiaxial loading. UEs calculated from only uniaxial loading trials were found to have a much larger MAD than those calculated from multiaxial trials. However, using both types of loading trials was found to be the most consistent between investigators. Future testing procedures should include a variety of both uniaxial and multiaxial loading trials, an example protocol could be as follows:

- 1) Varus-Valgus torque (applied until data has been collected through the full range of flexion, this should be assumed for all trials and takes approximately 60 to 90 seconds)
- 2) Internal-External torque
- 3) Anterior-Posterior force
- 4) Varus-Valgus + Internal torques (loads should be applied smoothly and together, rather than one after the other, this should be assumed for all multiaxial trials)
- 5) Varus-Valgus + External torques
- 6) Varus-Valgus torque + Anterior force
- 7) Varus-Valgus torque + Posterior force
- 8) Internal-External torque + Anterior force
- 9) Internal-External torque + Posterior force

The SDS method for calculating the UE has been shown to be an improvement over the previous method according to a variety of metrics. This method can be applied to future research involving the laxity of the passive knee joint and is likely general enough to be applied to research on the constraint of any joint. Applications may also be found in other work involving

RBFs, or the uncertainty associated with their approximations. Future work in this area could focus on creating total knee replacements that feel more like the natural knee, or a clinical device that estimate the UE *in vivo*.

References

- [1] Blankevoort, L., Huiskes, R., and de Lange, A., 1988, “The Envelope of Passive Knee Joint Motion,” *J. Biomech.*, **21**(9), pp. 705–720.
- [2] Hirschmann, M. T., and Müller, W., 2015, “Complex Function of the Knee Joint: The Current Understanding of the Knee,” *Knee Surgery, Sport. Traumatol. Arthrosc.*, **23**(10), pp. 2780–2788.
- [3] Mouton, C., Theisen, D., Meyer, T., Agostinis, H., Nührenbörger, C., Pape, D., and Seil, R., 2015, “Combined Anterior and Rotational Knee Laxity Measurements Improve the Diagnosis of Anterior Cruciate Ligament Injuries,” *Knee Surgery, Sport. Traumatol. Arthrosc.*, **23**(10), pp. 2859–2867.
- [4] Noyes, F. R., Cummings, J. F., Grood, E. S., Walz-Hasselfeld, K. A., and Wroble, R. R., 1991, “The Diagnosis of Knee Motion Limits, Subluxations, and Ligament Injury.,” *Am. J. Sports Med.*, **19**(2), pp. 163–71.
- [5] Bellemans, J., D’Hooghe, P., Vandenuecker, H., Damme, G. Van, and Victor, J., 2006, “Soft Tissue Balance in Total Knee Arthroplasty: Does Stress Relaxation Occur Perioperatively?,” *Clin. Orthop. Relat. Res.*, **452**(452), pp. 49–52.
- [6] Pugh, L., Mascarenhas, R., Arneja, S., Chin, P. Y. K., and Leith, J. M., 2009, “Current Concepts in Instrumented Knee-Laxity Testing,” *Am. J. Sports Med.*, **37**(1), pp. 199–210.
- [7] Torg, J. S., Conrad, W., and Kalen, V., 1976, “Clinical I Diagnosis of Anterior Cruciate Ligament Instability in the Athlete,” *Am. J. Sports Med.*, **4**(2), pp. 84–93.
- [8] Paessler, H. H., and Michel, D., 1992, “How New Is the Lachman Test?,” *Am. J. Sport. Med.*, **20**(1), pp. 95–98.
- [9] Benjaminse, A., Gokeler, A., and van der Schans, C. P., 2006, “Clinical Diagnosis of an

- Anterior Cruciate Ligament Rupture: A Meta-Analysis,” *J. Orthop. Sport. Phys. Ther.*, **36**(5), pp. 267–288.
- [10] Daniel, D. M., 1991, “Assessing the Limits of Knee Motion,” *Am. J. Sports Med.*, **19**(2), pp. 139–147.
- [11] Senioris, A., Rousseau, T., L’Hermette, M., Gouzy, S., Duparc, F., and Dujardin, F., 2017, “Validity of Rotational Laxity Coupled with Anterior Translation of the Knee: A Cadaveric Study Comparing Radiostereometry and the Rotab®,” *Knee*, **24**(2), pp. 289–294.
- [12] Hallén, L. G., and Lindahl, O., 1966, “The Screw-Home Movement in the Knee-Joint,” *Acta Orthop.*, **37**(1), pp. 97–106.
- [13] Markolf, K. L., Mensch, J. S., and Amstutz, H. C., 1976, “Stiffness and Laxity of the Knee--the Contributions of the Supporting Structures. A Quantitative in Vitro Study,” *J. Bone Joint Surg. Am.*, **58**(5), pp. 583–94.
- [14] Hsieh, H. H., and Walker, P. S., 1976, “Stabilizing Mechanisms of the Loaded and Unloaded Knee Joint,” *J. Bone Jt. Surg. - Ser. A*, **58**(1), pp. 87–93.
- [15] Chao, E. Y., Laughman, R. K., Schneider, E., and Stauffer, R. N., 1983, “Normative Data of Knee Joint Motion and Ground Reaction Forces in Adult Level Walking,” *J. Biomech.*, **16**(3), pp. 219–233.
- [16] Suntay, W. J., Grood, E. S., Hefzy, M. S., Butler, D. L., and Noyes, F. R., 1983, “Error Analysis of a System for Measuring Three-Dimensional Joint Motion,” *J. Biomech. Eng.*, **105**(2), p. 127.
- [17] Grood, E. S., and Suntay, W. J., 1983, “A Joint Coordinate System for the Clinical Description of Three-Dimensional Motions: Application to the Knee,” *J. Biomech. Eng.*,

- 105**(2), pp. 136–44.
- [18] Blankevoort, L., Huiskes, R., and de Lange, A., 1991, “Recruitment of Knee Joint Ligaments,” *J. Biomech. Eng.*, **113**(1), pp. 94–103.
- [19] Küpper, J. C., Loitz-Ramage, B., Corr, D. T., Hart, D. A., and Ronsky, J. L., 2007, “Measuring Knee Joint Laxity: A Review of Applicable Models and the Need for New Approaches to Minimize Variability,” *Clin. Biomech.*, **22**(1), pp. 1–13.
- [20] Pedersen, D., Vanheule, V., Wirix-Speetjens, R., Taylan, O., Delport, H. P., Scheys, L., and Andersen, M. S., 2018, “A Novel Non-Invasive Method for Measuring Knee Joint Laxity in 6-DOF: In Vitro Proof-of-Concept and Validation.”
- [21] Mane, A., 2007, “Combined Experimental and Statistical Model to Understand the Role of Anatomical and Implant Alignment Variables in Guiding Knee Joint Motion Combined Experimental and Statistical Model to Understand the Role of Anatomical and Implant Alignment Variables,” University of Kansas.
- [22] Clary, C. W., 2009, “A Combined Experimental-Computational Method to Generate Reliable Subject Specific Models of the Knee’s Ligamentous Constraint,” University of Kansas.
- [23] Cyr, A. J., 2014, “Quantification of the Relative Contribution of Individual Soft Tissue Structures to Total Joint Constraint,” University of Kansas.
- [24] Buhmann, M. D., and Levesley, J., 2004, *Radial Basis Functions: Theory and Implementations*.
- [25] Ahmed, S. G., and Mekey, M. L., 2010, “A Collocation and Cartesian Grid Methods Using New Radial Basis Function to Solve Class of Partial Differential Equations,” *Int. J. Comput. Math.*, **87**(6), pp. 1349–1362.

- [26] Cyr, A. J., and Maletsky, L. P., 2015, "Technical Note: A Multi-Dimensional Description of Knee Laxity Using Radial Basis Functions," *Comput. Methods Biomech. Biomed. Engin.*, **18**(15), pp. 1674–1679.
- [27] Leonard, J. A., Kramer, M. A., and Ungar, L. H., 1992, "Using Radial Basis Functions to Approximate a Function and Its Error Bounds," *IEEE Trans. Neural Networks*, **3**(4), pp. 624–627.
- [28] Maletsky, L. P., Sun, J., and Morton, N. A., 2007, "Accuracy of an Optical Active-Marker System to Track the Relative Motion of Rigid Bodies," *J. Biomech.*, **40**(3), pp. 682–685.
- [29] Lenz, N. M., 2008, "The Effects of Femoral Fixed Body Coordinate System Definition on Knee Kinematic Description," *J. Biomech. Eng.*, **130**(2), p. 021014.
- [30] Torzilli, P. A., Xianghua Deng, and Warren, R. F., 1994, "The Effect of Joint-Compressive Load and Quadriceps Muscle Force on Knee Motion in the Intact and Anterior Cruciate Ligament-Sectioned Knee," *Am. J. Sports Med.*, **22**(1), pp. 105–112.
- [31] Lewkonia, R. M., 1993, "The Biology and Clinical Consequences of Articular Hypermobility.," *J. Rheumatol.*, **20**(2), pp. 220–2.
- [32] Blankevoort, L., and Huiskes, R., 1996, "Validation of a Three-Dimensional Model of the Knee," *J. Biomech.*, **29**(7), pp. 955–961.
- [33] Mommersteeg, T. J. A., Huiskes, R., Blankevoort, L., Kooloos, J. G. M., Kauer, J. M. G., and Maathuis, P. G. M., 1996, "A Global Verification Study of a Quasi-Static Knee Model with Multi-Bundle Ligaments," *J. Biomech.*, **29**(12), pp. 1659–1664.
- [34] Malanga, G. A., Andrus, S., Nadler, S. F., and McLean, J., 2003, "Physical Examination of the Knee: A Review of the Original Test Description and Scientific Validity of Common Orthopedic Tests," *Arch. Phys. Med. Rehabil.*, **84**(4), pp. 592–603.

- [35] Cyr, A. J., and Maletsky, L. P., 2014, "Unified Quantification of Variation in Passive Knee Joint Constraint," *Proc. Inst. Mech. Eng. Part H J. Eng. Med.*, **228**(5), pp. 494–500.
- [36] Kwan, M. K., Lin, T. H.-C., and Woo, S. L.-Y., 1993, "On the Viscoelastic Properties of the Anteromedial Bundle of the Anterior Cruciate Ligament," *J. Biomech.*, **26**(4–5), pp. 447–452.
- [37] Cyr, A. J., Shalhoub, S. S., Fitzwater, F. G., Ferris, L. A., and Maletsky, L. P., 2015, "Mapping of Contributions From Collateral Ligaments to Overall Knee Joint Constraint: An Experimental Cadaveric Study," *J. Biomech. Eng.*, **137**(6), p. 061006.
- [38] Shultz, S. J., Shimokochi, Y., Nguyen, A. D., Schmitz, R. J., Beynnon, B. D., and Perrin, D. H., 2007, "Measurement of Varus-Valgus and Internal-External Rotational Knee Laxities in Vivo - Part I: Assessment of Measurement Reliability and Bilateral Asymmetry," *J. Orthop. Res.*, **25**(8), pp. 981–988.